Precision RNAi using synthetic shRNAmir target sites

Thomas Hoffmann[1,2,5,#], Alexandra Hörmann[3,#], Maja Corcokovic[3,#], Jakub Zmajkovic[1], Matthias Hinterndorfer[1], Jasko Salkanovic[3], Fiona Spreitzer[3], Anna Köferle[3], Katrin Gitschtaler[3], Alexandra Popa[3], Sarah Oberndorfer[3], Florian Andersch[1], Markus Schäfer[1], Michaela Fellner[1], Nicole Budano[3], Jan G. Ruppert[3], Paolo Chetta[3], Melanie Wurm[3], Johannes Zuber[1,4*] & Ralph A. Neumüller[3*]

[1] Institute of Molecular Pathology (IMP), Campus-Vienna-Biocenter 1, 1030 Vienna, Austria

[2] Vienna BioCenter PhD Program, Doctoral School of the University at Vienna and Medical University of Vienna, Vienna BioCenter (VBC), 1030 Vienna, Austria

[3] Boehringer Ingelheim RCV GmbH & Co KG, Doktor-Boehringer-Gasse 5-11, 1120 Vienna, Austria

[4] Medical University of Vienna, Vienna BioCenter, 1030 Vienna, Austria

[5] Present address: Advantage Therapeutics GmbH, Karl-Farkas-Gasse 22, 1030 Vienna, Austria

[#] These authors contributed equally to this work

[*] Corresponding authors: J.Z.: johannes.zuber@imp.ac.at; R.A.N.: ralph.neumueller@boehringer-ingelheim.com

Abstract

Loss-of-function genetic tools are widely applied for validating therapeutic targets, but their utility remains limited by incomplete on- and uncontrolled off-target effects. We describe artificial RNA interference (ARTi) based on synthetic, ultra-potent, off-target-free shRNAs that enable efficient and inducible suppression of any gene upon introduction of a synthetic target sequence into non-coding transcript regions. ARTi establishes a scalable loss-of-function tool with full control over on- and off-target effects.

Introduction

Drug development is guided by genetic loss-of-function (LOF) experiments that validate a therapeutic target, study its general and disease-specific functions, and thereby model and benchmark expected activities of inhibitory molecules. Applied genetic tools include RNAi, CRISPR/Cas9, and site-specific recombination technologies such as the Cre-Lox or Flp-FRT systems[1,2]. While these technologies have undoubtedly revolutionized genetic screening, target identification and validation, each method is associated with drawbacks that limit the usability for certain aspects of target validation. Specifically, RNAi is prone to off-target effects[3–5] and insufficient knock-down levels, while CRISPR/Cas9-based methods are associated with off-target effects and incomplete LOF across cell populations. These limitations are particularly problematic for candidate targets in oncology, which should ideally be validated genetically

in cancer cell lines and tumor models *in vivo*. In both cases, insufficient LOF or off-target effects can lead to far-reaching misconceptions about target suppression effects. Outgrowth of wild-type clones that retain gene function upon CRISPR- and recombination-based gene editing can result in transient phenotypes that complicate data interpretation. Similarly, insufficient knock-down or uncontrolled off-target effects induced by RNAi can lead to an unjustified de-prioritization or pursuit of candidate targets, respectively. Prior to initiating the time- and resource-intense process of drug development, more informative target validation assays would be highly desirable.

Results

To develop such an assay system, we reasoned that instead of using gene-specific LOF triggers for every new candidate gene, the expression of any gene could be efficiently suppressed by engineering the target site of a pre-validated, highly potent, synthetic short-hairpin RNA (shRNA) into its exonic sequence (Figure 1A). Besides ensuring efficient target knockdown in a highly standardized manner, such an approach would also provide control over off-target activities through expressing the shRNA side-by-side in target-site engineered and wildtype cells. This approach leaves the genome engineering procedure, needed to integrate the pre-validated artificial RNA interference (ARTi) target site into a gene of interest, as the only potential source of off-target effects. As suitable RNAi system, we chose optimized micro-RNA embedded shRNAs (shRNAmirs) in the miR-E backbone[6], which do not interfere with endogenous miRNA processing[7] and can be expressed from tet-responsive elements and other Pol-II promoters in the 3'-UTR of fluorescent reporter genes, thus providing a versatile system for inducible RNAi[8]. To identify potent ARTi sequences with minimal off-target activity, we analyzed the nucleotide composition of shRNAs that reach exceptionally high performance scores in common shRNA design algorithms[9] and of miRNA seed sequences with exceptionally low off-target scores according to siSPOTR[10]. By merging nucleotide biases identified in both analyses, we derived a 22-nt base composition matrix for the design of ARTi shRNAmirs (TTCGWWWNNAHHWWCATCCGGN; W = A/T, H = A/T/C; N = A/T/G/C) (Figure 1B; Figure 1 - figure supplement 1A,B). To further reduce possible off-target effects, we eliminated all shRNAs whose extended seed sequence (guide positions 2-14) had a perfect match in the human or mouse transcriptome and, finally, selected six top-scoring ARTi predictions for experimental validation.

We tested these ARTi-shRNAmirs using an established knockdown reporter assay[6] for their ability to suppress expression of a GFP transgene that harbors the respective target sites in its 3'-UTR. In all six cases, ARTi-shRNAmir matched or outperformed previously validated highly potent shRNAmirs targeting Renilla luciferase or PTEN[6] (Figure 1 - figure supplement 1C). We compared these results to a panel of 592 gene-specific shRNAs that were tested using the same assay and found that ARTi-shRNAmirs ranked among top-performing shRNAmirs overall (Figure 1C). Next, we selected the three top-performing ARTi-shRNAmirs and evaluated possible off-target activities using competitive proliferation assays and transcriptome profiling. ARTi-shRNAmir expression had no effects on proliferation or survival in four human and three mouse cell lines (Figure 1D; Figure 1 - figure supplement 1D), with the exception ARTi.6634 and ARTi.6786, which induced a mild fitness defect in the murine leukemia cell line RN2 and MV4-11 respectively. In contrast to effects of a MEK inhibitor trametinib, which we included as a positive control, stable expression of ARTi-shRNAmirs had only marginal effects on the transcriptome in two commonly used human cell lines (Figure 1E,F; Figure 1 - figure supplement 1E,F) and no effect in proliferation assays (Figure 1 - figure supplement 1G), indicating that they do not trigger major off-target

effects, even in the absence of their respective target site. Together, these studies established a set of highly potent, off-target-free ARTi-shRNAmirs, among which we selected ARTi.6570 (ARTi-shRNAmir) for further investigations.

To establish ARTi as a method for target validation, we performed ARTi-based LOF experiments in cancer cell lines and xenograft models for three prominent oncology targets: EGFR and KRAS, which act as driving oncogenes in various cancer types[11,12], and STAG1, which has been identified as a synthetic lethal interaction with recurrent LOF mutations of STAG2[13–16]. To establish an ARTi-repressible version of oncogenic EGFR^{del19}, we cloned ARTi-shRNAmir target sequences into an expression construct encoding EGFR^{del19} fused to dsRed (Figure 2A), which rendered Ba/F3 cells cytokine-independent and sensitive to EGFR inhibition (Figure 2 – figure supplement 2A). We introduced this construct into human EGFR^{del19}-dependent PC-9 lung adenocarcinoma cells and subsequently knocked out the endogenous *EGFR* gene. The EGFR^{del19}::V5::dsRed::ARTi transgene fully rescued the loss of endogenous EGFR^{del19}, while doxycycline (dox)-induced expression of the ARTi-shRNAmir (ARTi.6570) strongly inhibited proliferation of PC-9 cells and triggered a near-complete suppression of the EGFR^{del19}::V5::dsRed::ARTi protein (Figure 2B,C; Figure 2 – figure supplement 2B). Consistently, in RNA-sequencing we observed an almost complete drop of reads mapping to the codon-optimized *EGFR^{del19}::V5::dsRed::ARTi* transgene upon dox-inducible expression of the ARTi-shRNAmir, as well as a downregulation of *DUSP6* and other canonical targets of RAF-MEK-ERK signaling, which acts as key effector pathway of EGFR^{del19} (Figure 2 – figure supplement 2C-E).

To evaluate whether ARTi can recapitulate drug activities *in vivo*, we xenotransplanted *EGFR^{del19}::V5::dsRed::ARTi* engineered PC-9 cells harboring the dox-inducible ARTi-shRNAmir and treated recipient mice upon tumor formation with either dox or the clinically approved EGFR inhibitor Osimertinib. Dox-induced expression of the ARTi-shRNAmir led to rapid and durable tumor regression that was indistinguishable from the effects of Osimertibib (Figure 2d) and not observed in parental PC-9 cells that lack the ARTi target site (Figure 2 – figure supplement 2F). We therefore conclude that ARTi-induced phenotypes are to be attributed to on-target effects that predict the activity of advanced small-molecule inhibitors *in vivo*.

In a second study, we used ARTi to investigate KRAS^{G12R}, an oncogenic KRAS variant with no available *in-vivo* compatible inhibitors. To establish a suitable KRAS^{G12R}-driven model, we engineered a *dsRed::KRAS^{G12R}-ARTi* transgene and the dox-inducible ARTi-shRNAmir into KRAS^{G12C}-dependent MIA PaCa-2 pancreatic adenocarcinoma cells and subsequently knocked out endogenous *KRAS* alleles (Figure 2E; Figure 2 – figure supplement 3A). As expected, switching the driving oncogene from KRAS^{G12C} to KRAS^{G12R} rendered MIA PaCa-2 cells resistant to the KRAS^{G12C} inhibitor AMG-510[17–19] (Figure 2 – figure supplement 3B). ARTi-shRNAmir induction led to strong suppression of dsRed::KRAS^{G12R} expression at the mRNA and protein level (Figure 2F; Figure 2 – figure supplement 3C,D) and marked anti-proliferative effects (Figure 2G). In xenograft experiments, ARTi-mediated suppression of KRAS^{G12R} led to full tumor regression in the absence of KRAS^{G12C} (Figure 2H), while tumors harboring both oncogenic KRAS alleles only displayed a delay in tumor progression, suggesting that both oncogenes contribute to tumor growth *in vivo*.

To evaluate STAG1 as synthetic-lethal dependency that is relevant in wide range of STAG2-deficient cancers (Figure 2 – figure supplement 4A)[13–16], we engineered an isogenic pair of STAG2-wildtype and -deficient HCT 116 colon carcinoma cells and homozygously inserted ARTi target sites (besides an AID::V5

tag; explained in the materials and methods section) into the 3'-UTR of endogenous *STAG1* (Figure 2I). Western blotting confirmed the knockout of *STAG2*, the insertion of the targeting cassette into the *STAG1* locus, and potent suppression of STAG1 following dox-induced ARTi-shRNAmir expression (Figure 2J,K; Figure 2 – figure supplement 4B). Suppression of STAG1 in STAG2-deficient HCT 116 cells impaired their proliferation *in vitro* (Figure 2 – figure supplement 4C) and the progression of xenografted tumors *in vivo* (Figure 2L), while dox-induced expression of the ARTi-shRNAmir had no anti-proliferative effects in the presence of STAG2.

Discussion

Together, these studies establish ARTi as a versatile and precise LOF method for target validation in oncology and beyond. Instead of designing gene-specific LOF reagents that remain prone to off-target effects, ARTi involves a simple, highly standardized experimental procedure that provides full control over on- and off-target effects and can be applied to any coding and non-coding gene. In cells that are pre-engineered to express the dox-inducible ARTi-shRNAmir, candidate genes can be converted into ARTi target genes and subsequently evaluated head-to-head in a highly standardized manner, either through knocking in ARTi target sites into endogenous loci or through knock-out rescue approaches. Placement of ARTi target sites in non-coding transcript regions leaves the endogenous target protein unaltered, which is a key advantage over chemical-genetic LOF methods relying on the introduction of degron tags[20,21]. Targeting endogenously engineered ARTi target sites through tetracycline (Tet)-inducible ARTi-shRNAmir expression enables inducible, titratable, and likely reversible (not tested in this study) LOF perturbations of candidate genes without altering their endogenous transcriptional regulation, which is not possible using conventional Tet-expression systems. In principle, by engineering multiple target sites in the same cell, ARTi enables combinatorial LOF perturbations, e.g. for modeling synergistic target interactions, without multiplying the risk for off-target effects. Although ARTi requires the design of gene-specific sgRNAs and genome engineering steps that can be non-trivial, the method enables researchers to reach well-interpretable, comparable, and unambiguous experimental results that can guide larger investments in targets of high medical interest. Beyond providing a scalable method for early target validation, we foresee that ARTi can be used to establish on-target benchmark phenotypes for guiding the development and optimization of inhibitory molecules.

Figure Legends

Figure 1: Design and selection ARTi-shRNAmirs. A, Schematic outline of the ARTi approach. **B,** Sequence logo (https://weblogo.berkeley.edu) displaying nucleotide position biases of 2161 shRNAs with exceptionally high DSIR scores (>105). Inlay depicts miRNA seed sequence biases. **C,** Reporter assay comparing gene-specific shRNAs to ARTi-shRNAmirs. **D,** Competitive proliferation assays in human cell lines after transduction with ARTi-shRNAmirs, neutral (shRen.713) and essential control shRNAs (shRPL9.324 or shPSMA3.164). **E,** Principal component (PC) analysis of gene expression profiling upon stable expression of indicated shRNAs or treatment with MEK inhibitor (trametinib) in RKO cells. **F,**

159 Volcano plots visualizing de-regulated genes upon expression of indicated shRNAs and trametinib
160 treatment in RKO cells, compared to empty vector control.

161

162 **Figure 2: Experimental validation of the ARTi approach. A,** Schematic of EGFR^{del19}::V5::dsRed::ARTi
163 engineering in PC-9 cells. Blue color denotes overexpressed ARTi variant. Green denotes endogenous
164 gene. **B,** Western Blot demonstrating knock-down of EGFR^{del19}::V5::dsRed::ARTi. Western Blot is a
165 representative example of three independent biological repeat experiments. **C,** Proliferation assay and
166 crystal violet staining of parental and engineered PC-9 cells in absence or presence of dox. Crystal violet
167 staining is a representative example of two independent biological repeat experiments. **D,** *In vivo*
168 experiment comparing dox-induced EGFR^{del19}::V5::dsRed::ARTi knockdown to pharmacological EGFR^{del19}
169 inhibition. Mean tumor volume and +/- s.e.m. is plotted for all *in vivo* experiments. **E,** Schematic of MIA
170 PaCa-2 engineering. Blue color denotes overexpressed ARTi variant. Green denotes endogenous gene. **F,**
171 Western blot for KRAS and Actin in indicated engineered MIA PaCa-2 cells in the presence and absence of
172 dox. Western Blot is a representative example of two independent biological repeat experiments. **G,**
173 Proliferation assay and crystal violet staining of parental and engineered MIA PaCa-2 cells in absence or
174 presence of dox. Crystal violet staining is a representative example of two independent biological repeat
175 experiments. **H,** Growth curves of tumors implanted with engineered MIA PaCa-2 cells in absence and
176 presence of dox. In vivo **I,** Schematic of C-terminal endogenous tagging of STAG1. Green color denotes
177 endogenous genes. **J,** Western Blot demonstrating knock-down of STAG1-ARTi. Western Blot is a
178 representative example of three independent biological repeat experiments. **K,** Immunohistochemistry
179 staining of STAG1 in engineered HCT 116 cells in absence and presence of dox. Asterisk marks an area of
180 murine fibroblasts that serve as an internal positive control. **I,** Growth curves of tumors implanted with
181 engineered HCT 116 cells in the absence and presence of dox.

182

183 **Figure 1 – figure supplement 1: Design and selection ARTi-shRNAmirs. A,** Sequence logo displaying
184 nucleotide position biases of seed sequences (guide position 2-8) with the lowest off-target score in
185 siSPOTR analysis (top 1%). **B,** Sequence logo displaying position biases in sequences from a that harbor a
186 T in guide position 2. **C,** Knockdown efficiency of ARTi-shRNAmirs. Flow cytometric quantification of GFP
187 knockdown efficiency in immortalized MEFs two days after transduction with indicated ARTi-shRNAmir or
188 control shRNAs. Percent knockdown is normalized to shRen.713 control. shRen.660 served as a neutral
189 control whose target site was not included in the reporter. Red asterisks indicate ARTi-shRNAmirs that
190 were selected for follow-up studies. **D,** Toxicity of ARTi-shRNAmirs. Competitive proliferation assays of
191 three murine cell lines after transduction with ARTi-shRNAmirs, shRen.713 or shMyc.1834 control,
192 showing the relative fraction of shRNA-expressing cells at indicated time points following the initial
193 measurement (day 4 after shRNA transduction). **E,** Principal component analysis of gene expression
194 profiling in HT-1080 cells. Respective shRNAmirs and treatments are indicated in the respective colors. X-
195 axis: principal component 1; Y-axis: principal component 2. **F,** Volcano plots visualizing de-regulated genes
196 in HT 1080 cells. All shRNAmirs and treatments were tested against the empty vector control. X-axis: -
197 $\log_{10}$(p-value); Y-axis: $\log_2$ fold change. **G,** Cell growth assay for ARTi-shRNAmir transduced cells and their
198 parental controls in the presence and absence of dox.

199

200 **Figure 2 – figure supplement 1: Validation of ARTi *in vitro* and *in vivo* - EGFR. A,** Functional validation of
201 the $EGFR^{del19}$ construct in Ba/F3 cells. Provided are GI_{50} values (nM) for indicated conditions and
202 compounds (parental cells IL-3 dependent; other cells dependent on transgenes (no IL-3)). Numbers
203 represent GI_{50} value calculated from three technical repeats. Three biological repeat experiments were
204 conducted, and one representative experiment is shown in panel A. **B,** Western Blot analysis confirming
205 expression of $EGFR^{del19}$::V5::dsRed::ARTi constructs, knockout of endogenous EGFR and dox-induced
206 knockdown or $EGFR^{del19}$::V5::dsRed::ARTi. Western Blot is a representative example of three
207 independent biological repeat experiments. **C,** Expression levels (y-axis: normalized counts) of the
208 $EGFR^{del19}$::V5::dsRed::ARTi construct in parental and engineered PC-9 cells after 4 and 8 days of dox
209 treatment or no treatment. Individual datapoints of three biological replicates overlay the boxplots. **D,**
210 Expression levels (y-axis: normalized counts) of the MAPK target gene *DUSP6* in parental and engineered
211 PC-9 cells after 4 and 8 days of dox treatment or no treatment. Individual datapoints of three biological
212 replicates overlay the boxplots. **E,** Heatmap visualizing the gene expression changes in MAPK pathway
213 target and ERBB genes in engineered cells in the presence and absence of dox. **F,** *In vivo* experiment
214 comparing dox-induced expression of the ARTi-shRNAmir to drinking water control in PC-9 parental
215 cells. Lines connect mean tumor volume data and +/- s.e.m..

216

217 **Figure 2 – figure supplement 2: Validation of ARTi *in vitro* and *in vivo* - KRAS. A,** Schematic of MIA PaCa-
218 2 genome engineering. **B,** AMG-510 GI_{50} values in MIA PaCa-2 parental and engineered cells. Numbers
219 represent GI_{50} value calculated from three technical repeats. Three biological repeat experiments were
220 conducted, and one representative experiment is shown in panel B. **C,** Expression levels (y-axis:
221 normalized counts) of the dsRed::$KRAS^{G12R}$ transgene in parental and engineered MIA PaCa-2 cells after 4
222 and 8 days of dox treatment or no treatment. Individual datapoints of three biological replicates overlay
223 the boxplots. **D,** Western blot for KRAS (green) and Actin (magenta) (upper plot) and dsRed (green) and
224 Actin (magenta) (bottom plot) for indicated engineered MIA PaCa-2 cells in the presence and absence of
225 dox. Western Blot is a representative example of three independent biological repeat experiments.

226

227 **Figure 2 – figure supplement 3: Validation of ARTi *in vitro* and *in vivo* – STAG1. A,** Schematic of synthetic
228 lethal interaction between STAG1 and STAG2. Cells survive loss of either paralog but are incapable of
229 growing upon combined loss of STAG1 and STAG2. **B,** Western blot confirmation of STAG2 knockout and
230 ARTi-shRNAmir induced knockdown of endogenous STAG1::V5::ARTi. Western Blot is a representative
231 example of three independent biological repeat experiments. **C,** Proliferation assay of ARTi engineered
232 HCT 116 cells *in vitro*, visualized by crystal violet staining following a 9-day dox or control treatment.
233 Staining is a representative example of three independent biological repeat experiments. **D**,
234 Quantification of nuclear Stag1 level (Figure 2k) using engineered HCT 116 cells in an in vivo
235 xenotransplantation experiment the control group (-dox) and doxycycline (+dox) treated group.

236 **Figure 2 – source data 1.** Original blots for Figure 2B and Figure2 - figure supplement 1B.

237 **Figure 2 – source data 2.** Original blots for Figure 2F.

238 **Figure 2 – source data 3.** Original blots for Figure 2J.

239 **Figure 2 – figure supplement 2 – source data 1.** Original blots for Figure2 - figure supplement 2D.

240 **Figure 2 – figure supplement 3 – source data 1.** Original blots for Figure2 - figure supplement 3B.

241

242 Material and Methods

243 Design and cloning of ARTi shRNAs

244 To design pairs of artificial shRNAs and matching target sites that trigger effective and selective target
245 suppression with minimal off-target effects, nucleotide composition of shRNAs that reach exceptionally
246 high performance scores in a well-established siRNA prediction tool (DSIR=Designer of Small Interfering
247 RNA[9]) and contain no A or T in guide position 20 to eliminate shRNAmirs that produce RISC-loadable small
248 RNAs from the passenger strand were analyzed. To establish criteria for ARTi design, siRNA predictions
249 for the human and mouse genome were retrieved from DSIR[9] using default parameters. Top scoring
250 predictions (DSIR score > 105) harboring G or C in position 20 were analyzed for nucleotide biases, which
251 were used to define basic design criteria at the 5'-end the 3'-half. Next, possible off-targets were
252 minimized using siSPOTR[10], an siRNA-based prediction tool that assesses off-target potential of different
253 siRNA seed sequences (guide positions 2-8) in the human and mouse genome. Seed sequences with the
254 lowest predicted off-target activity (top 1%) showed biases for C and/or G in guide positions 2-6, but 23%
255 contained a T at the 5' end of the seed sequence that is required in our design (Fig. 1b). Among these, we
256 observed particularly strong biases for CG in the following two positions (Fig. 1b), which were found in
257 73% of all seed sequences harboring a 5' T. Overall, 17% of all top-scoring seed sequences harbored TCG
258 at their 5' end, making it the second most common triplet (after CGC, which was found in 20%). Based on
259 these analyses, we fixed the first 4 nucleotides of the guide to TTCG. For the following positions we
260 reasoned that introducing additional GC biases would destroy 5'-3' asymmetry of small RNA duplexes that
261 is critically required for efficient RISC loading. To maintain sufficient asymmetry, we therefore decided to
262 bias the next 3 positions towards A or T, which in most positions is in alignment with nucleotide biases
263 associated with knockdown efficacy.

264 For the remaining sequence 3' of the seed region, we adhered to nucleotide features associated with
265 knockdown efficacy based on our DSIR analysis, which are remarkably prominent and cannot all be
266 explained through established processing requirements. Altogether, this established a 22-nt matrix for
267 the design of ARTi shRNAmirs (TTCGWWWNNAHHWWCATCCGGN; W = A/T, H = A/T/C; N = A/T/G/C). In a
268 last step, we further reduced possible off-target effects by eliminating all guides whose extended seed
269 sequence (guide positions 2-14) had a perfect match in the human or mouse transcriptome and, finally,
270 selected the following six top-scoring ARTi predictions for experimental validation:

271 ARTi.6588 – target site: TCCGGATGAAGTTTATATCGAA / shRNAmir (97mer):
272 TGCTGTTGACAGTGAGCGCCCGGATGAAGTTTATATCGAATAGTGAAGCCACAGATGTATTCGATATAAACTTCAT
273 CCGGATGCCTACTGCCTCGGA

274 ARTi.6570 – target site: TCCGGATGATATTGTTATCGAA / shRNAmir (97mer):
275 TGCTGTTGACAGTGAGCGCCCGGATGATATTGTTATCGAATAGTGAAGCCACAGATGTATTCGATAACAATATCAT
276 CCGGATGCCTACTGCCTCGGA

277 ARTi.6634 – target site: TCCGGATGATGTTTTAATCGAA / shRNAmir (97mer):
278 TGCTGTTGACAGTGAGCGCCCGGATGATGTTTTAATCGAATAGTGAAGCCACAGATGTATTCGATTAAAACATCAT
279 CCGGATGCCTACTGCCTCGGA

280 ARTi.6786 – target site: TCCGGATGATATTGTATACGAA / shRNAmir (97mer):
281 TGCTGTTGACAGTGAGCGCCCGGATGATATTGTATACGAATAGTGAAGCCACAGATGTATTCGTATACAATATCAT
282 CCGGATGCCTACTGCCTCGGA

283 ARTi.6834 – target site: TCCGGATGATATTGCATACGAA / shRNAmir (97mer):
284 TGCTGTTGACAGTGAGCGCCCGGATGATATTGCATACGAATAGTGAAGCCACAGATGTATTCGTATGCAATATCAT
285 CCGGATGCCTACTGCCTCGGA

286 ARTi.6516 – target site: TCCGGATGAAGTTTAATTCGAA / shRNAmir (97mer):
287 TGCTGTTGACAGTGAGCGCCCGGATGAAGTTTAATTCGAATAGTGAAGCCACAGATGTATTCGAATTAAACTTCAT
288 CCGGATGCCTACTGCCTCGGA

289

290 The following ARTi target sequences were used for experimental validation studies:

291 Insertion into the coding sequence before the STOP codon:

292 ATCCGGATGATATTGTATACGAATCCGGATGATATTGTTATCGAA (with the first "A" being inserted to retain
293 the reading frame)

294 Insertion after the STOP codon:

295 TCCGGATGATATTGTATACGAATCCGGATGATGTTTTAATCGAATCCGGATGATATTGTTATCGAA

296 shRNAs were ordered as single stranded DNA Ultramer oligonucleotides (Integrated DNA Technologies),
297 amplified by PCR and cloned into different retroviral or lentiviral miRE/miRF shRNAmir expression vectors
298 (LT3GFPIR[6]) using EcoR/XhoI restriction digest or Gibson assembly.

299

300 **Cell Culture**

301 Human HCT 116 cells (ATCC: CCL-247) were cultured in RPMI 1640 medium (Thermo Fisher) and PC-9 cells
302 in McCoy's 5A medium (Thermo Fisher), supplemented with 10% FBS and 1 x GlutaMAX (Thermo Fisher).
303 RKO (ATCC: CRL-2577) and MOLM-13 cells (DSMZ: ACC 584) were cultured in RPMI 1640, supplemented
304 with 10% FBS (Sigma-Aldrich), 4mM L-glutamine (Thermo Fisher), 1mM sodium pyruvate (Sigma-Aldrich),
305 and penicillin/streptomycin (100 U ml^{-1}/100 µg ml^{-1}, Sigma-Aldrich). HT-1080 (ATCC: CCL-121) and LentiX
306 lentiviral packaging cells (Clontech, cat. no. 632180) were cultivated in DMEM (Thermo Fisher) with 10%
307 FBS, 4mM L-glutamine, 1mM sodium pyruvate, and penicillin/streptomycin (100 U ml^{-1}/100 µg ml^{-1}).
308 MV4-11 cells (ATCC: CRL-9591) were cultured in IMDM with 10% FBS, 4mM L-glutamine, 1mM sodium
309 pyruvate, and penicillin/streptomycin (100 U ml^{-1}/100 µg ml^{-1}).

310 Murine MLL-AF9^{OE}, Nras^{G12D} AML cells (RN2; Zuber et al. 2011) were cultured in RPMI 1640 medium
311 supplemented with 10% FBS, 20 mM L-glutamine, 10 mM sodium pyruvate, 10 mM HEPES (pH 7.3),
312 penicillin/streptomycin (100 U ml^{-1}/100 µg ml^{-1}), and 50 µM β-ME. *Kras^{G12D}*, *Trp53$^{-/-}$*, *MYC^{OE}* PDAC cells
313 (EPP2), SV40 large T antigen immortalized mouse embryonic fibroblasts (RRT-MEF[22]; and NIH/3T3 (ATCC:
314 CRL-1658) were cultured in DMEM supplemented with 10% FBS, 20 mM glutamine, 10 mM sodium
315 pyruvate, and penicillin/streptomycin (100 U ml^{-1}/100 µg ml^{-1}). MIA PaCa-2 (ATCC: CRL-1420) and GP2d
316 (Ecacc: 95090714) cells were cultured in DMEM supplemented with 10% FBS. Ba/F3 (DSMZ: ACC300) cells
317 were cultured in RPMI 1640 medium supplemented with 10% FBS, 10ng/ml IL-3 (R&D systems) and Ls513

318 cells were cultured in RPMI 1640 medium supplemented with 10% FBS. All cell lines were maintained at
319 37°C with 5% CO_2, routinely tested for mycoplasma contamination and authenticated by short tandem
320 repeat analysis.

321

322 **Reporter Assay**

323 SFFV-GFP-P2A-Puro-ARTi-target sensor was cloned into pRSF91 retroviral plasmid[23] using Gibson
324 assembly. RRT-MEFs were transduced with retroviruses expressing a GFP-reporter harboring the target
325 sites for validated shRNAs and one ARTi-shRNA in its 3'-UTR. For each reporter cell line single cells were
326 FACS-sorted into 96-well plates using a FACSAria III cell sorter (BD Bioscience) to obtain single-cell derived
327 clones. These clones were transduced with retrovirus constructs in pSin-TRE3G-mCherry-miRE-PGK-Neo
328 (TCmPNe) backbone expressing either the respective doxycycline (dox)-inducible ARTi shRNA or validated
329 shRNAs and mCherry fluorescence marker. shRNA expression was induced with dox and GFP levels were
330 quantified via flow cytometry 2 days post induction. Knockdown efficiency was calculated as 1 minus the
331 ratio of mean GFP signal in $mCherry^+$ ($shRNA^+$) cells over $mCherry^-$ cells and normalized to Renilla
332 luciferase specific neutral control shRNA (Ren.713).

333

334 **Competitive proliferation assay**

335 To investigate the effect of ARTi constructs in the absence of the endogenous target gene, competitive
336 proliferation assays were performed in several human and murine cell lines. Human HT-1080, RKO,
337 MOLM-13, and MV4-11 cell lines were lentivirally transduced with shRNAmir expression constructs cloned
338 into pRRL-SFFV-GFP-miRF-PGK-Neo (SGFN) backbone at 20-60% efficiency. Initial infection efficiency was
339 determined at day 4 post transfection (day 0) by measuring GFP expression as a readout using iQue
340 Screener Plus flow cytometer (IntelliCyt). Percentage of $shRNA^+$ cells (GFP positive) was monitored by flow
341 cytometry in regular intervals and results were normalized to day 0.

342 Human GP2d, Ls513, and MIA PaCa-2 cell lines were lentivirally transduced with shRNAmir constructs
343 cloned into pRRL-TRE3G-GFP-miRE-PGK-Puro-IRES-rtTA3 backbone (LT3GEPIR, Addgene plasmid
344 #111177). 500 cells were seeded in duplicates in 96-well plates and treated with 1 µg/ml dox for 9-10 days
345 and analyzed with Incucyte (Sartorius). Untreated cells served as reference.
346 Murine NIH-3T3, EPP2 and RN2 cells were retrovirally transduced with shRNAmir constructs cloned into
347 pMSCV-miR-E-PGK-Neo-IRES-mCherry backbone (LENC; Addgene plasmid #111163), and initial infection
348 levels were determined by flow cytometry based on mCherry expression 4 days post transduction (day 0).
349

350 **Crystal Violet staining**

351 To visualize ARTi-shRNAmir's effect, crystal violet staining assays were performed. 25'000 HCT 116 cells
352 and 15'000 PC-9 cells per well were seeded in a 6-well plate containing 2 mL tetracycline-free growth
353 medium and 1 µg/mL dox. Medium was exchanged every 2-3 days. After 9 days, wells were washed with
354 ice-cold PBS and subsequently stained with 1 mL of 2.3% crystal violet solution for 10 minutes.
355 Subsequently, wells were washed with ultrapure water and dried overnight. Images were obtained with
356 a scanner.

357
358
359 **Transcriptional profiling**

360 For the unbiased identification of ARTi shRNA off-targets, RKO and HT-1080 shRNA$^+$ cells from the
361 competition proliferative assay experiment were selected with Geneticin/G418 Sulfate (Gibco) for 7 days
362 and checked for GFP expression. On day 7, one arm of the empty vector control group was treated with
363 IC_{50} concentration of trametinib (MedChem Express: HY-10999) for 24 hours based on the data in
364 Genomics of Drug Sensitivity in Cancer (GDSC) database (https://www.cancerrxgene.org)[24]. Subsequently,
365 cells were trypsinized, washed with ice-cold PBS, pelleted and snap frozen. Total RNA was isolated using
366 in-house magnetic beads kit and King Fisher Duo Prime Purification System (Thermo Fisher). NGS libraries
367 were prepared with QuantSeq 3' mRNA-Seq Library Prep Kit (FWD) HT for Illumina (Lexogen) and UMI
368 Second Strand Synthesis Module for QuantSeq FWD (Lexogen). Samples were sequenced on Illumina
369 NovaSeq platform with 100bp single-read protocol.

370 Engineered MIA PaCa-2 and PC-9 cells were cultured in the presence of 1 µg/ml dox to induce expression
371 of the ARTi shRNA. dox-containing media were replenished twice weekly and on day 4 and day 8 after the
372 initial treatment. $2x10^6$ dox-treated and untreated control cells were harvested, washed with PBS, lysed,
373 treated with DNAse I (QIAGEN) and total RNA was extracted using the RNeasy Mini Kit (QIAGEN). NGS
374 libraries were prepared as above. Samples were sequenced on an Illumina NextSeq 2000 platform with a
375 75bp protocol.
376
377 **Bioinformatic analyses of 3' mRNA-Seq**

378 For 3' mRNA-Seq reads derived from the human cell lines HT-1080 and RKO, the six nucleotide long 5'
379 UMIs were attached to each read name with umi-tools (v1.0.0)[25]. Subsequently, the UMIs plus the next
380 four nucleotides (UMI spacer), as well as 3' adapters (stringency of 3) and bases with low quality (threshold
381 of 25) were trimmed away using cutadapt (v1.18)[26] and its wrapper tool trimgalore (v0.6.2). Read quality
382 control was performed with FastQC (v0.11.8). The remaining reads were sample-wise aligned to the
383 human (GRCh38.p13; GCA_000001405.28) reference genome. Mapping and subsequent filtering of 3' UTR
384 mapped reads was performed with slamdunk (v0.4.3)[27] in QuantSeq mode (slamdunk map -5 12 -n 100 -
385 q). 3' UTR regions were assembled based on the description in Muhar et al.[28]. Aligned and filtered reads
386 were deduplicated with umi-tools (v1.0.0) (2), based on the mapping coordinate and the UMI attached to
387 the read name, prior to quantifying read abundances within 3' UTR regions using featureCounts (v2.0.1)[29].
388 Differential expression analysis (DEA) was performed with DESeq2 (v1.30.1)[30] for each ARTi shRNA to
389 empty vector control. Here, the number of up- and downregulated genes were calculated by filtering the
390 DEA results for genes with a log2 fold-change ≥ 2 (up) or ≤ 2 (down) and a -log10 p-value ≥ 5. Principal
391 component analysis was performed on the 1000 most variable expressed genes with the prcomp function
392 from the stats (v4.2.0) R package.

393 For transcriptional profiling of the human cell lines MIA PaCa-2 and PC-9, the genome reference file and
394 annotations were constructed based on the GRCh38 assembly and the Ensembl 86 version, respectively.
395 The sequences of the shRNA construct (ARTi.6570 (RN_v_76, RN_v_118)) as well as the

396 EGFR^{del19}::V5::dsRed::ARTi (RN_v_108) and the dsRed::Linker::KRAS^{G12R}-ARTi (RN_v_287) were also
397 included. Mapping of the sequencing reads derived from the human cell lines was performed with STAR
398 (v2.5.2b)[31] aligner allowing for soft clipping of adapter sequences. Quantification of read counts to
399 transcript annotations was implemented using RSEM (v1.3.0)[32] and featureCounts (v1.5.1)[29].
400 Normalization of read counts and differential analysis was implemented with the limma[33] and voom[34] R
401 packages.
402
403 **Genome engineering of EGFR in PC-9 and Ba/F3**

404 Genome engineering of PC-9 cells was done as previously described[35]. In brief: PC-9_RIEN cells were
405 transduced with an ecotropic pMSCV-EGFRdel19_V5_dsRed_ARTi-PGK-Blasticidin retrovirus cloned at
406 GenScript and produced in Platinum E cells (Cell Biolabs) in the presence of 8 µg/mL Polybrene (Merck
407 Millipore). After 24 hours, stable transgenic cell pools were selected using 10 µg/mL Blasticidin (Sigma-
408 Aldrich). Subsequently, cells were diluted to obtain single cell clones. After 14 days of culture, single cell-
409 derived colonies were transferred to 6-well plates and analyzed by Western Blot. Identified homozygous
410 PC-9_ EGFR^{del19}-ARTi clones were further engineered by cutting endogenous EGFR with a CRISPR all-in-
411 one vector pX458_Exon20_gRNA `TAGTCCAGGAGGCAGCCGAA` (GenScript) using X-tremeGENE 9 DNA
412 transfection reagent (Roche) according to the protocol supplied by the vendor. 48 hours after
413 transfection, GFP positive cells were sorted by FACS (SONY cell sorter S800Z) and diluted to obtain single
414 cell clones. Positive clones, which contained only the exogenous EGFR^{del19}-ARTi, but not the endogenous
415 EGFR, were identified by Western Blot. Next, the selected EGFR clone was transduced with a pantropic
416 LT3GEPIR_Puro_ARTi-shRNA `TTCGATAACAATATCATCCGGA` retrovirus cloned at GenScript, China and
417 produced via the Lenti-X Single Shot system (Clontech). 72 hours later, stable transgenic cell pools were
418 selected using 0.5µg/mL Puromycin (Sigma-Aldrich). Following the selection, cells were diluted to obtain
419 single cell clones. After 14 days of culture, single cell-derived colonies were transferred to 6-well plates
420 and induced via 1µg/ mL dox. Positive clones were characterized by a strong GFP-induction that was
421 identified by flow cytometry.

422

423 Ba/F3 cells were transduced with an ecotropic pMSCV-EGFRdel19_V5_dsRed_ARTi-PGK-Blasticidin
424 retrovirus cloned at GenScript and produced in Platinum E cells in the presence of 4 µg/mL Polybrene.
425 After 72 hours, stable transgenic cells were selected by using 50 µg/mL Blasticidin, without adding IL-3.
426

427 **Genome engineering of KRAS in MIA PaCa-2**

428 MIA PaCa-2 ARTi-shRNAmir expressing cells were transduced with an ecotropic pMSCV-dsRed::KRAS^{G12R}-
429 ARTi-PGK-Blasticidin retrovirus cloned at GenScript, China and produced in Platinum E cells in the
430 presence of 8 µg/mL Polybrene. After 24 hours, stable transgenic cell pools were selected using 10 µg/mL
431 Blasticidin. Subsequently, endogenous KRAS was knocked out by transient transfection of three gRNAs
432 targeting exon 2 and the region containing the G12C variant (present in MIA PaCa-2 cells) were used in a
433 co-transfection (gRNA#3: *GAATATAAACTTGTGGTAGT*; gRNA#6: *CTTGTGGTAGTTGGACTTG*; gRNA#7:
434 *GTAGTTGGAGCTTGTGGCGT*). Knockout clones were identified by the absence of the endogenous KRAS
435 protein using Western Blot.

436

437 **Genome engineering of STAG1/STAG2 in HCT 116**

438 HCT 116 cell line was engineered by cutting STAG1 with gRNAs targeting the region close to the STOP
439 codon. Guide RNAs *TTCTTCAGACTTCAGAACAT* or *CTGAAGAAAATTTACAAATC* were cloned into the
440 pSpCas9(BB)-2A-GFP plasmid (pX458; Addgene plasmid 48138) and used in a co-transfection.
441 Simultaneously, a STAG1_AID_V5_P2A_Blasti_STOP_ARTi repair template with 800bp of left and right
442 homologous arms of the STAG1 genomic locus (in pUC57-Simple backbone) was transfected into HCT 116
443 cells using Lipofectamine 3000 transfection reagent (Thermo Fisher) according to the manufacturer's
444 instructions. A stable transgenic cell pool was selected 48 hours after transfection using 5µg/ml Blasticidin
445 and diluted to obtain single cell clones. Positive clones were identified by Western Blot.

446 Identified homozygous HCT 116_STAG1_ARTi clones were further engineered by disrupting STAG2 gene
447 with a CRISPR all-in-one vector Hs0000077505_U6gRNA-Cas9-2A-GFP and Hs0000077502_U6gRNA-Cas9-
448 2A-GFP, respectively. Cells were transfected using X-tremeGENE 9 DNA transfection reagent according to
449 the manufacturer's instructions, sorted 48 hours post transfection for GFP positive cells and diluted to
450 obtain single cell clones. Positive clones were identified by Western Blot.

451 Next, the selected HCT 116 clone was transduced with a pantropic LT3GEPIR_Puro_ARTi-shRNA
452 *TTCGATAACAATATCATCCGGA* retrovirus cloned at GenScript, China and produced via the Lenti-X Single
453 Shot system (Clontech). 72 hours later, stable transgenic cell pools were selected using 2 µg/mL Puromycin
454 (SIGMA, P9620). Following the selection, cells were diluted to obtain single cell clones. After 14 days of
455 culture, single cell-derived colonies were transferred to 6-well plates and induced via 1µg/ mL dox.
456 Positive clones were characterized by a strong GFP-induction that was identified by flow cytometry.
457

458 **Western Blot**

459 The following primary antibodies were used for immunoblot analyses: EGFR (Cell Signaling, #4267); STAG1
460 (GeneTex, GTX129912); STAG2 (Bethyl, A300-159A); b-actin (Sigma, A5441); KRAS (LSbio, LS-C17566); V5
461 (Sigma, V8012). PC-9, MIA PaCa-2, and HCT 116 cell pellets harboring EGFR, KRAS, and STAG1/STAG
462 constructs respectively were lysed in Triton X-100 lysis buffer, sonicated and stored at -80°C. For protein
463 detection, the pellets were thawed on ice, followed by 15 minutes centrifugation at 13,000 rpm and 4°C.
464 Further, cell lysates were loaded onto a pre-casted SDS–polyacrylamide gel (4-12%) and proteins were
465 transferred onto a nitrocellulose or PVDF-membrane. Membranes were probed with the respective
466 primary antibodies overnight. The next day, secondary antibodies conjugated with fluorescent dye were
467 added and the proteins were detected by the Odyssey detection system.
468

469 **Compound treatment**

470 To investigate sensitivity to EGFR-targeting compounds, cell viability was determined using the Cell Titer
471 Glo assay (Promega). For this purpose, 10 mM stock solutions in DMSO of afatinib[36], Osimertinib[37,38] [37]
472 and poziotinib[39,40] were used. 5'000 cells per well were seeded in 150µL of the medium in technical
473 triplicates in 96-well plates and incubated at 37°C and 5% CO_2 for 5 hours, followed by the compound
474 addition. Cells were treated with seven different concentrations of inhibitors in a serial eight-fold dilutions
475 starting with the highest concentration of 3 µM. For comparability, DMSO normalization to the highest
476 added volume was performed. Subsequently, cells were cultivated for 96 hours at 37°C and 5% CO_2. 50 µL
477 of Cell Titer Glo reagent was added to each well, incubated for 10 minutes in the dark and luminescence

478 was measured using the multilabel Plate Reader VICTOR X4. The measurement time was set to 0.2
479 seconds. Luminescence values relative to DMSO-treated cells were plotted in GraphPad Prism and fitted
480 using nonlinear regression with a variable slope to calculate IC50 values at 50% inhibition. MIA PaCa-2
481 KRAS G12C inhibitor (AMG-510)[17–19] treatments were performed as described for EGFR with the following
482 modifications: 2'000 cells per well, and 0.5nM-3µM concentration range of AMG-510.

483

484 ***In vivo* experiments**

485 The PC-9 EGFR k.o., EGFR^{del19}::ARTi study was performed at the AAALAC accredited animal facility of
486 CrownBio Leicestershire, UK. Female NSG® (NOD.Cg-PrkdcscidIl2rgtm1wjl/SzJ) Crl mice were obtained
487 from Charles River. Age of animals at study initiation was 7-8 weeks and hat an acclimatization period of
488 ≥14 days. Mice were groups housed in IVCs. The study complies with the UK Animals Scientific Procedures
489 Act 1986 (ASPA) in line with Directive 2010/63/EU of the European Parliament and the Council of 22
490 September 2010 on the protection of animals used for scientific purposes.

491 All other in vivo experiments were performed at the AAALAC accredited animal facility of Boehringer
492 Ingelheim RCV GmbH & CoKG. Female BomTac:NMRI-*Foxn1^{nu}* mice were obtained from Taconic Denmark
493 at 6-8 weeks of age. After the arrival, mice were allowed to adjust to the housing conditions at least for 5
494 days before the start of the experiment. Mice were housed in pathogen-free and controlled
495 environmental conditions (open cage housing), and handled according to the institutional, governmental
496 and European Union guidelines (Austrian Animal Protection Laws, GV-SOLAS and FELASA guidelines).

497 Studies were approved by the internal ethics committee (called "ethics committee") of Boehringer
498 Ingelheim RCV GmbH & Co KG in the department of Cancer Pharmacology and Disease Positioning.
499 Furthermore, all protocols were approved by the Austrian governmental committee (MA 60 Veterinary
500 office; approval numbers GZ: 903122/2017/21 and GZ: 416181-2020-29).

501 To establish subcutaneous tumors, mice were injected with 2 x 10^6 HCT 116 in PBS, 5 x 10^6 MIA PaCa-2
502 in 1:2 Matrigel : PBS with 5% FBS or with 1 x 10^7 PC-9 cells in PBS with 5% FBS.

503 Tumor diameters were measured with a caliper three times a week. The volume of each tumor [in mm^3]
504 was calculated according to the formula "tumor volume = length * diameter^2 * π/6." Mice were
505 randomized into the treatment groups when tumor size reached between ~130 and 190 mm^3. Group sizes
506 were calculated for each tumor model based on tumor growth during model establishment experiments.
507 A power analysis was performed using a sample size calculator
508 (https://www.stat.ubc.ca/~rollin/stats/ssize/n2.html). For all models used in the studies, 10 mice per
509 group were used. 2mg/ml doxycycline hyclate (Sigma) and 5mg/ml sucrose were added to the drinking
510 water of the treatment groups, the control group received water with 5mg/ml sucrose only. Osimertinib
511 (Tagrisso, AstraZeneca, 40 mg tablet) was dosed per os daily at a dose of 25mg/kg in Natrosol and control
512 mice were dosed per os daily with Natrosol. To monitor side effects of treatment, mice were inspected
513 daily for abnormalities and body weight was determined three times per week. Animals were sacrificed
514 when the tumors reached a size of 1'500 mm^3. Food and water were provided ad libitum. *In vivo*
515 experiments were not repeated.

516

517 **Immunohistochemistry**

518 Xenograft samples were fixed in 4% formaldehyde for 24 h and embedded in paraffin. Two-micrometer-
519 thick sections were cut using a microtome. STAG1 was stained with Polink 2 Plus HRP rat NM detection
520 system (GBI Labs #D46-6) according to manufacturer's instructions using a recombinant rat monoclonal
521 STAG1 antibody (Abcam ab241544, Lot:GR3334172-1; 1:200) after cooking 10 minutes at 110°C in
522 antigen unmasking solution (Vector #H3301). After staining the slides were digitalized (scanner: Leica
523 Aperio AT2). All slides were reviewed and evaluated for quality by a board-certified MD Pathologist.
524 Imaging analysis was performed using the digital pathology platform HALO (Indica Labs). A tissue-
525 classifying algorithm was trained to selectively recognize viable tumor tissue against stroma, necrosis,
526 and skin. The tissue classification output for each scan was reviewed and manually edited as necessary.
527 A cell detection and scoring algorithm was trained to measure DAB optical density (OD) in the nuclei of
528 tumor cells. A positivity threshold for DAB OD was determined by normalization with respect to the DAB
529 OD as calculated from *bona fide* negative tissue (e.g., murine stroma as background). The object data for
530 background-normalized nuclear ODs for each tumor cell were exported from three control and three
531 doxycycline-treated cases (207945 and 33331 pooled objects, respectively). The cumulative distribution
532 of the background-normalized DAB OD for each tumor cell nucleus was then plotted for control and
533 doxycycline-treated cases, separately (supplemental figure 4, panel K).

534

535 **Reagents, code and data availability**

536 DNA sequences of the transgenes used in this study and the code used to generate the figures are
537 available upon request. The workflow for the RNA-seq bioinformatics analyses is described in the
538 Materials and Methods section. RNA sequencing data were uploaded to GEO with the accession
539 numbers: GSE218404 and GSE218617. The data will be made publicly available upon acceptance of this
540 manuscript. All ARTi cell lines and constructs described in this study are available upon request.

541

542 **Cell lines**

543 All newly generated ARTi cell lines are available upon request. The following parental cell lines were
544 used:

545

Cell line name	species	Supplier name	Catalog number	Clone number
PC-9	human	ECACC	90071810	Lot# 14A030
MIA PaCa-2	human	ATCC	CRL-1420	Lot# 1350798
HT 1080	human	ATCC	CCL-121	Lot# 63835574
HCT 116	human	ATCC	CCL-247	Lot# 6028631
RKO	human	ATCC	CRL-2577	Lot# 59354083
MV4-11	human	ATCC	CRL-9591 (old number)	Lot# 58352230
MOLM-13	human	DSMZ	ACC 554	Lot# 11
NIH-3T3	human	ATCC	CRL-1658	Lot# 63292276
EPP2		KrasG12D, Trp53-/-, MYCOE PDAC cells (EPP2)	NA	NA

RN2	murine	MLL-AF9OE, NrasG12D AML cells (RN2; Zuber et al. 2011)	NA	NA
Gp2d	human	ECACC	95090714	Lot# 11E013
Ls513	human	ATCC	CRL-2134	Lot# 57761342
Ba/F3	murine	DSMZ	ACC300	
293T-Lenti-X	human	Clontech	632180	Lot# 1404558A

Competing interests

Alexandra Hörmann, Maja Corcokovic, Jasko Salkanovic, Fiona Spreitzer, Anna Köferle, Katrin Gitschtaler, Alexandra Popa, Sarah Oberndorfer, Nicole Budano, Jan G. Ruppert, Paolo Chetta, Melanie Wurm and Ralph Neumüller: Are or were full time employees Boehringer Ingelheim. Johannes Zuber: Quantro Therapeutics GmbH (Co-founder, Scientific Advisor, Shareholder); Mirimus Inc. (Scientific Advisor, Shareholder); AstraZeneca-CRUK Functional Genomics Consortium (Scientific Advisor); Boehringer Ingelheim (Research Support).

Funding

J.Z. is supported by the Swiss National Science Foundation (Early Postdoc Mobility Fellowship P2BSP3_188110) and European Union's Horizon 2020 research and innovation program under the Marie Skłodowska-Curie grant agreement No. 847548 (VIP2) and No. 101032582 (AML-SynergyX). Research at the IMP is supported by Boehringer Ingelheim and the Austrian Research Promotion Agency (Headquarter grant FFG-852936). MS is a member of the Boehringer Ingelheim Discovery Research global post-doc program.

Acknowledgements

The authors thank all colleagues in the labs of Johannes Z. and R.A.N. for critical discussions and technical support.

566 ## References

567

568 1. Mohr, S. E., Smith, J. A., Shamu, C. E., Neumüller, R. A. & Perrimon, N. RNAi screening comes of age:
569 improved techniques and complementary approaches. *Nat Rev Mol Cell Bio* 15, 591–600 (2014).

570 2. Housden, B. E. *et al.* Loss-of-function genetic tools for animal models: cross-species and cross-
571 platform differences. *Nat Rev Genet* 18, 24–40 (2017).

572 3. Jackson, A. L. *et al.* Expression profiling reveals off-target gene regulation by RNAi. *Nat Biotechnol* 21,
573 635–637 (2003).

574 4. Scacheri, P. C. *et al.* Short interfering RNAs can induce unexpected and divergent changes in the levels
575 of untargeted proteins in mammalian cells. *P Natl Acad Sci Usa* 101, 1892–1897 (2004).

576 5. Lin, X. *et al.* siRNA-mediated off-target gene silencing triggered by a 7 nt complementation. *Nucleic*
577 *Acids Res* 33, 4527–4535 (2005).

578 6. Fellmann, C. *et al.* An Optimized microRNA Backbone for Effective Single-Copy RNAi. *Cell Reports* 5,
579 1704–1713 (2013).

580 7. Premsrirut, P. K. *et al.* A Rapid and Scalable System for Studying Gene Function in Mice Using
581 Conditional RNA Interference. *Cell* 145, 145–158 (2011).

582 8. Zuber, J. *et al.* Toolkit for evaluating genes required for proliferation and survival using tetracycline-
583 regulated RNAi. *Nat Biotechnol* 29, 79–83 (2011).

584 9. Vert, J.-P., Foveau, N., Lajaunie, C. & Vandenbrouck, Y. An accurate and interpretable model for siRNA
585 efficacy prediction. *Bmc Bioinformatics* 7, 520 (2006).

586 10. Boudreau, R. L. *et al.* siSPOTR: a tool for designing highly specific and potent siRNAs for human and
587 mouse. *Nucleic Acids Res* 41, e9–e9 (2013).

588 11. Hynes, N. E. & MacDonald, G. ErbB receptors and signaling pathways in cancer. *Curr Opin Cell Biol*
589 21, 177–184 (2009).

590 12. Punekar, S. R., Velcheti, V., Neel, B. G. & Wong, K.-K. The current state of the art and future trends in
591 RAS-targeted cancer therapies. *Nat Rev Clin Oncol* 1–19 (2022) doi:10.1038/s41571-022-00671-9.

592 13. Bailey, M. L. *et al.* Paralogous synthetic lethality underlies genetic dependencies of the cancer-
593 mutated gene STAG2. *Life Sci Alliance* 4, e202101083 (2021).

594 14. Lelij, P. van der *et al.* STAG1 vulnerabilities for exploiting cohesin synthetic lethality in STAG2-
595 deficient cancers. *Life Sci Alliance* 3, e202000725 (2020).

596 15. Benedetti, L., Cereda, M., Monteverde, L., Desai, N. & Ciccarelli, F. D. Synthetic lethal interaction
597 between the tumour suppressor STAG2 and its paralog STAG1. *Oncotarget* 5, 37619–37632 (2014).

598 16. Lelij, P. van der *et al.* Synthetic lethality between the cohesin subunits STAG1 and STAG2 in diverse
599 cancer contexts. *Elife* 6, e26980 (2017).

600 17. Fakih, M. *et al.* CodeBreak 100: Activity of AMG 510, a novel small molecule inhibitor of KRAS G12C ,
601 in patients with advanced colorectal cancer. *J Clin Oncol* 38, 4018–4018 (2020).

602 18. Lanman, B. A. *et al.* Discovery of a Covalent Inhibitor of KRASG12C (AMG 510) for the Treatment of
603 Solid Tumors. *J Med Chem* 63, 52–65 (2020).

604 19. Fakih, M. *et al.* Phase 1 study evaluating the safety, tolerability, pharmacokinetics (PK), and efficacy
605 of AMG 510, a novel small molecule KRAS G12C inhibitor, in advanced solid tumors. *J Clin Oncol* 37,
606 3003–3003 (2019).

607 20. Lai, A. C. & Crews, C. M. Induced protein degradation: an emerging drug discovery paradigm. *Nat Rev*
608 *Drug Discov* 16, 101–114 (2017).

609 21. Cromm, P. M. & Crews, C. M. Targeted Protein Degradation: from Chemical Biology to Drug
610 Discovery. *Cell Chem Biol* 24, 1181–1190 (2017).

611 22. Fellmann, C. *et al.* Functional Identification of Optimized RNAi Triggers Using a Massively Parallel
612 Sensor Assay. *Mol Cell* 41, 733–746 (2011).

613 23. Galla, M. *et al.* Avoiding cytotoxicity of transposases by dose-controlled mRNA delivery. *Nucleic Acids*
614 *Res* 39, 7147–7160 (2011).

615 24. Yang, W. *et al.* Genomics of Drug Sensitivity in Cancer (GDSC): a resource for therapeutic biomarker
616 discovery in cancer cells. *Nucleic Acids Res* 41, D955–D961 (2013).

617 25. Smith, T., Heger, A. & Sudbery, I. UMI-tools: modeling sequencing errors in Unique Molecular
618 Identifiers to improve quantification accuracy. *Genome Res* 27, 491–499 (2017).

619 26. Martin, M. Cutadapt removes adapter sequences from high-throughput sequencing reads. *Embnet J*
620 17, 10–12 (2011).

621 27. Neumann, T. *et al.* Quantification of experimentally induced nucleotide conversions in high-
622 throughput sequencing datasets. *Bmc Bioinformatics* 20, 258 (2019).

623 28. Muhar, M. *et al.* SLAM-seq defines direct gene-regulatory functions of the BRD4-MYC axis. *Science*
624 360, 800–805 (2018).

625 29. Liao, Y., Smyth, G. K. & Shi, W. featureCounts: an efficient general purpose program for assigning
626 sequence reads to genomic features. *Bioinformatics* 30, 923–930 (2014).

627 30. Love, M. I., Huber, W. & Anders, S. Moderated estimation of fold change and dispersion for RNA-seq
628 data with DESeq2. *Genome Biol* 15, 550 (2014).

629 31. Dobin, A. *et al.* STAR: ultrafast universal RNA-seq aligner. *Bioinformatics* 29, 15–21 (2013).

630 32. Li, B. & Dewey, C. N. RSEM: accurate transcript quantification from RNA-Seq data with or without a
631 reference genome. *Bmc Bioinformatics* 12, 323 (2011).

632 33. Ritchie, M. E. *et al.* limma powers differential expression analyses for RNA-sequencing and
633 microarray studies. *Nucleic Acids Res* 43, e47–e47 (2015).

634 34. Law, C. W., Chen, Y., Shi, W. & Smyth, G. K. voom: precision weights unlock linear model analysis
635 tools for RNA-seq read counts. *Genome Biol* 15, R29–R29 (2014).

636 35. Wilding, B. *et al.* Discovery of potent and selective HER2 inhibitors with efficacy against HER2 exon
637 20 insertion-driven tumors, which preserve wild-type EGFR signaling. *Nat Cancer* 3, 821–836 (2022).

638 36. Li, D. *et al.* BIBW2992, an irreversible EGFR/HER2 inhibitor highly effective in preclinical lung cancer
639 models. *Oncogene* 27, 4702–4711 (2008).

640 37. Liu, S. *et al.* Targeting HER2 Aberrations in Non–Small Cell Lung Cancer with Osimertinib. *Clin Cancer*
641 *Res* 24, 2594–2604 (2018).

642 38. Soria, J.-C. *et al.* Osimertinib in Untreated EGFR -Mutated Advanced Non–Small-Cell Lung Cancer.
643 *New Engl J Med* 378, 113–125 (2018).

644 39. Kim, T.-Y. *et al.* A phase I/II study of poziotinib combined with paclitaxel and trastuzumab in patients
645 with HER2-positive advanced gastric cancer. *Gastric Cancer* 22, 1206–1214 (2019).

646 40. Robichaux, J. P. *et al.* Pan-Cancer Landscape and Analysis of ERBB2 Mutations Identifies Poziotinib as
647 a Clinically Active Inhibitor and Enhancer of T-DM1 Activity. *Cancer Cell* 36, 444-457.e7 (2019).

648

Design and selection of ARTi-shRNAmirs

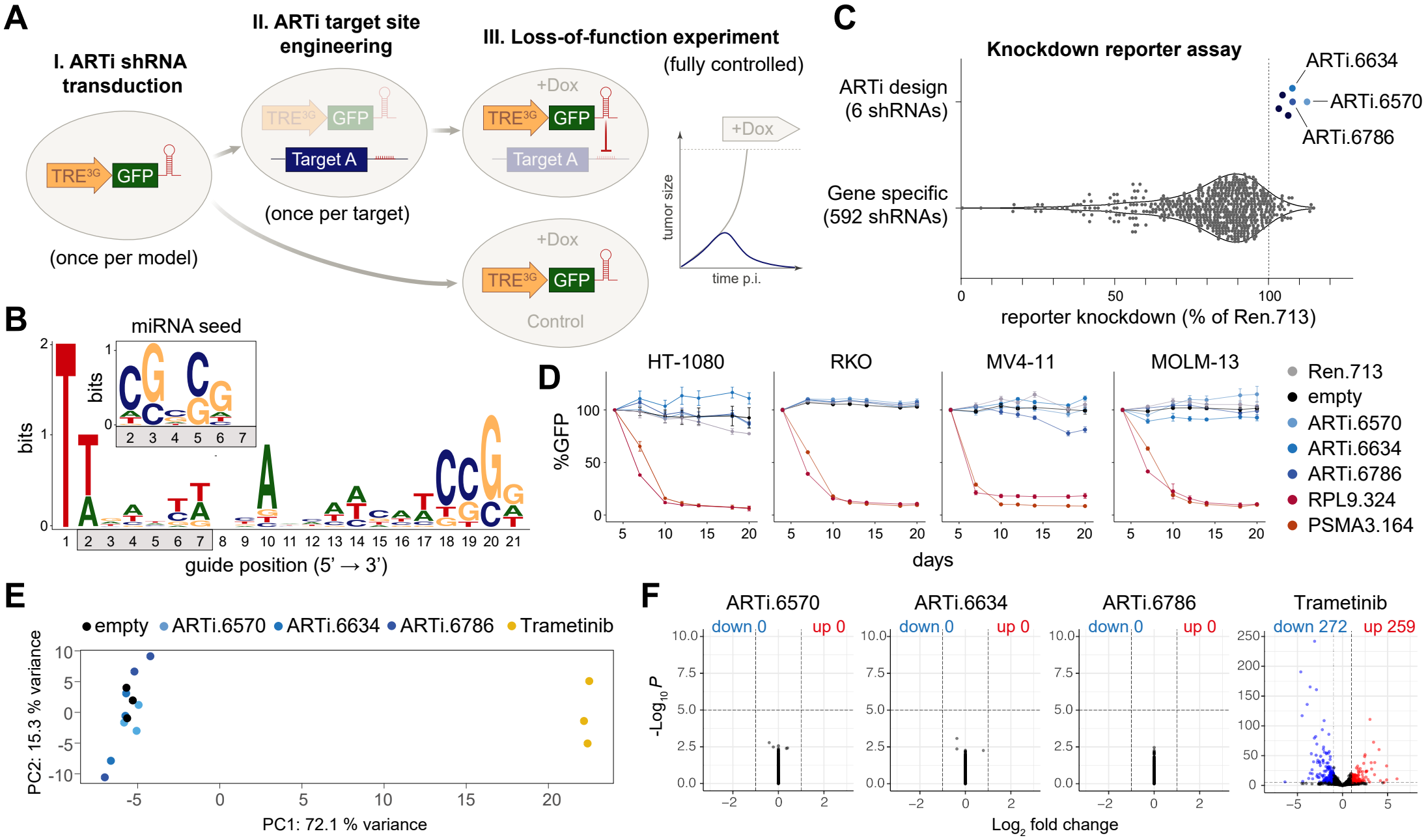

Hoffmann et al., Figure 1

Experimental validation of the ARTi approach

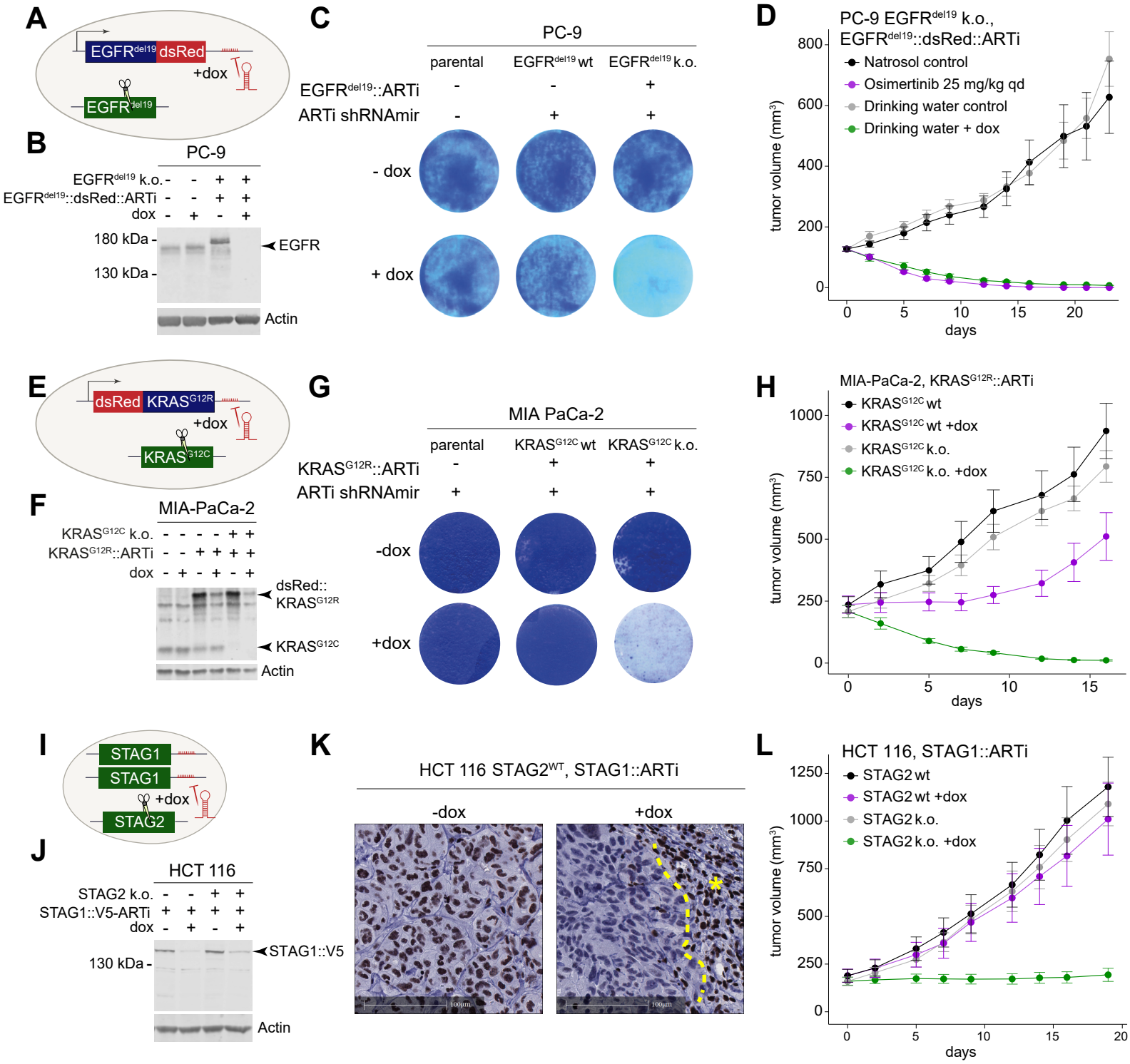

Hoffmann et al., Figure 2